Probing the Solid Phase of Noble Metal Copper at Terapascal Conditions

D. E. Fratanduono,[1,*] R. F. Smith,[1] S. J. Ali,[1] D. G. Braun,[1] A. Fernandez-Pañella,[1] S. Zhang,[1] R. G. Kraus,[1] F. Coppari,[1] J. M. McNaney,[1] M. C. Marshall,[1] L. E. Kirch,[1] D. C. Swift,[1] M. Millot,[1] J. K. Wicks,[2] and J. H. Eggert[1]

[1]*Lawrence Livermore National Laboratory, Livermore, California 94550, USA*

[2]*Department of Earth and Planetary Sciences, Johns Hopkins University, Baltimore, Maryland 21218, USA*

(Received 28 February 2019; revised manuscript received 22 July 2019; published 8 January 2020)

Ramp compression along a low-temperature adiabat offers a unique avenue to explore the physical properties of materials at the highest densities of their solid form, a region inaccessible by single shock compression. Using the National Ignition Facility and OMEGA laser facilities, copper samples were ramp compressed to peak pressures of 2.30 TPa and densities of nearly 30 g/cc, providing fundamental information regarding the compressibility and phase of copper at pressures more than 5 times greater than previously explored. Through x-ray diffraction measurements, we find that the ambient face-centered-cubic structure is preserved up to 1.15 TPa. The ramp compression equation-of-state measurements shows that there are no discontinuities in sound velocities up to 2.30 TPa, suggesting this phase is likely stable up to the peak pressures measured, as predicted by first-principal calculations. The high precision of these quasiabsolute measurements enables us to provide essential benchmarks for advanced computational studies on the behavior of dense monoatomic materials under extreme conditions that constitute a stringent test for solid-state quantum theory. We find that both density-functional theory and the stabilized jellium model, which assumes that the ionic structure can be replaced by an ionic charge distribution by constant positive-charge background, reproduces our data well. Further, our data could serve to establish new international secondary scales of pressure in the terapascal range that is becoming experimentally accessible with advanced static and dynamic compression techniques.

DOI: 10.1103/PhysRevLett.124.015701

With the advent of high-energy-density facilities [1–3], the field of high-energy-density physics has seen rapid growth of experimental techniques able to access regions of the phase space that was previously inaccessible. Large-scale laser facilities [1,3] and pulsed power machines [2], have demonstrated the ability to quasi-isentropically compress materials to extreme conditions (> 0.5 TPa). These facilities now routinely measure the off-Hugoniot equation of state (EOS) of materials to precisions that were previously only achievable along the principal Hugoniot [4–7]. These advancements in ramp compression and x-ray diffraction experiments now enable the benchmarking and testing of theoretical predictions at pressure-temperature conditions found within Jovian cores [6]. To understand the nature of solids at extreme compression, it is first best to examine materials that are predicted to have no phase transition and simple band structure.

Copper, as well as gold and silver, are deemed noble metals, defined as materials that have a single valence electron and nearly spherical Fermi surface. The Fermi surface for the noble metals has a single branch that can adequately be treated as one-band metals in the calculation of their thermodynamic properties. In these materials, a smooth variation of the density as a function of pressure over large compression is predicted. Studying the isentropic pressure-density response of a simple noble metal compressed to threefold compression is an excellent test of first-principal calculations and the equation-of-state model.

Historically, EOS tables have been based upon shock Hugoniot data and isothermal data from diamond anvil cell (DAC) experiments. Density-functional theory (DFT) then provides constraints on how the empirically constrained models should extrapolate beyond the generally limited compression range of current techniques ($\sim$0.6 TPa for dynamic compression and $\sim$0.2 TPa for DAC). To date, accurate high-pressure (> 0.5 TPa) experimental constraints of the cold curve have been limited. Ramp-compression techniques offer a unique avenue to test DFT calculations and benchmark EOS tables at unprecedented pressure conditions. We determine pressure, density, and sound speed along a continuous adiabatic compression path to 2.30 TPa. Using x-ray diffraction techniques, we examine the crystal structure to 1.15 TPa in order to test first-principal structural predictions.

Ramp-compression experiments to determine the isentropic response were conducted at the National Ignition Facility (NIF) located at the Lawrence Livermore National Laboratory. NIF can deliver up to 2 MJ of laser energy over 30 ns and provide the necessary laser power and control to ramp compress materials to > 1 TPa pressures [6,7]. The target design to ramp compress Cu to 2.30 TPa consists of a stepped sample with four thicknesses,

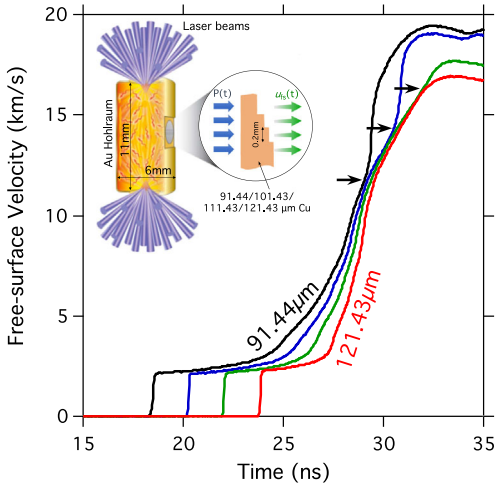

FIG. 1. The measured free-surface velocity as a function of time $u_{\mathrm{fs}}(t)$ determined from VISAR [8]. The extracted $u_{\mathrm{fs}}(t)$ profiles are shown for Cu thicknesses of 91.44 (black), 101.43 (blue), 111.43 (green), and 121.43 μm (red). Arrows on individual step profiles indicate the arrival of a reverberation wave, which results in a secondary acceleration and analysis termination. (Inset) The target design is shown. A multistepped copper physics package is mounted on the equator of 11 × 6-mm hohlraum.

91/101/111/121 μm (Fig. 1, inset). The energy from 176 laser beams was converted by a hohlraum into an x-ray drive which, through direct ablation, imparted an initial steady shock followed by a monotonically increasing ramp pressure wave into the sample. By measuring how the wave profiles steepen as a function of thickness, the sound speed, and hence the stress-density response of the material is determined [4–7].

A Doppler velocity interferometer known as a velocity interferometer system for any reflector [8] (VISAR) was used to measure the time history of the Cu free-surface velocity $u_{\mathrm{fs}}(t)$ for each of the four Cu thicknesses (Fig. 1). The VISAR system images across the Cu steps in one dimension with ~30-μm spatial resolution and provides continuous velocity versus time data over a 1-mm field of view. Two VISAR channels with different velocity sensitivities were used simultaneously to resolve any velocity ambiguities that could arise if the rate of target velocity change exceeded the time response of the system. A total of six ramp-compression experiments were performed with an initial shock states ranging from 10 to 73 GPa.

For each shot, a noniterative Lagrangian analysis [9–12] to determine *in situ* particle velocities was used to translate $u_{\mathrm{fs}}(t)$ data (from all four Cu thicknesses) into Lagrangian sound speed [$C_L(u_p)$, where u_p is the particle velocity]. The initial shock state is modeled using the experimentally measured Hugoniot with linear extrapolation of the $C_L(u_p)$ response to zero pressure to properly model the subsequent centered rarefaction. The $C_L(u_p)$ data for six shots are shown in Fig. 2(a). $C_L(u_p)$ and its uncertainty $\sigma_{C_L}(u_p)$ are obtained from thickness and velocity versus time data by

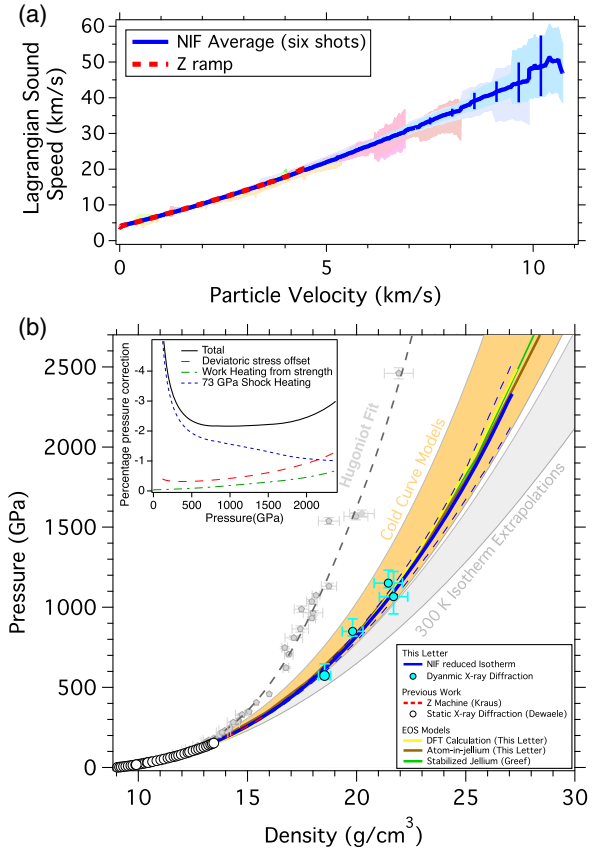

FIG. 2. (a) Lagrangian sound velocity C_L versus particle velocity u_p was calculated from u_{fs} versus sample thickness data (Fig. 1). Six experiments, each with two independent velocity measurements, yielded $C_L(u_p)$ data and their averages (bold blue curve) are shown. (b) Experimentally determined pressure-density data along an isentrope to 2.30 TPa are shown as the bold blue curve with dashed blue lines representing 1-σ bounding uncertainties. We also show a previous low-pressure measurement of Cu isentrope (red dashed line) [5], a range of calculated cold curves [13–21], and extrapolations from low-pressure 300-K static compression data (white circles) [22]. Our x-ray diffraction points along a ramp-compressed path are shown as light blue symbols. (Inset) We illustrate the percent correction applied to reduce the measured stress-density response to a hydrostatic pressure-density isentrope.

linear regression using errors determined by our measurement accuracies. $C_L(u_p)$ and $\sigma_{C_L}(u_p)$ are integrated to obtain $P_x = P_H + \rho_0 \int_{u_{p,H}}^{u_p} C_L du_p$ and $\rho = ([1/\rho_H] - [1/\rho_0] \times \int_{u_{p,H}}^{u_p} [du_p/C_L])^{-1}$ and their uncertainties $\sigma_{P_x}^2 = \sigma_{P_{x,H}}^2 + (\rho_0 \int_{u_{p,H}}^{u_p} \sigma_{C_L} du_p)^2$ and $\sigma_\rho^2 = ([\rho_H^2/\rho_0^2]\delta\rho_H)^2 + ([\rho^2/\rho_0] \times \int_{u_H}^{u_p} [\sigma_{C_L}/C_L^2] du_p)^2$. Here P_H, ρ_H, and $u_{p,H}$ are the pressure, density, and particle velocity, respectively, associated with the initial shock Hugoniot state. Uncertainties are propagated though the integrals linearly, rather than in quadrature because they appear to be strongly correlated rather than random. This method of uncertainty propagation allows the direct propagation of experimental uncertainties. A total of

six NIF experiments are shown in Fig. 2(a) with different color bands and the average of all six experiments is shown in blue.

In these experiments, we measure the longitudinal stress σ_x. Under uniaxial strain conditions, the longitudinal stress can be separated into a hydrostatic component (P_{hyd}) and a stress deviator term. Assuming the von Mises criterion, the longitudinal stress is defined as $\sigma_x = P_{\mathrm{hyd}} + \frac{2}{3}Y$, where Y is the yield strength. For solid materials with strength, the stress deviators cause plastic work heating, a source of thermal pressure. The thermal pressure difference between the hydrostat and the isentrope due to plastic work heating is defined as $P_{\mathrm{hyd}} - P_{\mathrm{isen}} = \gamma\rho \int_0^{\varepsilon_x} \beta dW_P$, where γ is the Grüneisen parameter, ε_x is the natural strain $\log(\rho/\rho_o)$, β is the Taylor-Quinney factor taken to be 0.9 for copper [5], and W_p is the plastic work heating. The pressure along the isentrope is now defined as $P_{\mathrm{isen}} = \sigma_x - \frac{2}{3}Y - \gamma\rho \int \beta dW_p$.

To achieve high-pressure states in these experiments, it was necessary to first shock compress the copper sample. To reduce the longitudinal stress measurements to the principal isentrope, it is also necessary to account for the initial shock state. We utilize the Grüneisen parameter to relate pressure states between the Hugoniot and isentrope: $P_{\mathrm{Hug}} - P_{\mathrm{isen}} = \gamma\rho_{\mathrm{Hug}}(E_{\mathrm{Hug}} - E_{\mathrm{isen}})$. To reduce our measurements (σ_x) to the principal isentrope, we solve $P_{\mathrm{isen}} = \sigma_x - \frac{2}{3}Y - \gamma\rho \int \beta dW_p - \gamma\rho_{\mathrm{Hug}}(E_{\mathrm{Hug}} - E_{\mathrm{isen}})$. To perform this correction, we require a model for the high-pressure Grüneisen parameter [$\gamma(\rho)$], the differential amount of plastic work heating (dW_p), and the yield strength.

For the Grüneisen parameter, we utilize the Al'tshuler form from Kraus *et al.* [5] for compressions (ρ_0/ρ) between 1 and 0.64. Below a compression of 0.64, the Mie-Grüneisen relation between the Hugoniot and isentrope is used to determine the Grüneisen parameter as a function of density. As in Kraus *et al.* [5], this is done iteratively, as the calculation requires pressure and internal energy along the isentrope. The differential plastic work heating is defined as [23] $dW_P = (1/\rho_0)\frac{2}{3}Y[d\varepsilon_x - dY/2G(\rho)]$, where $G(\rho)$ is the shear modulus. We utilized a scaled Steinberg-Guinan strength model to determine $G(\rho)$ and the resulting yield strength. The application of systematic corrections as a function of pressure to our experimentally determined P_x-ρ path is shown in the inset to Fig. 2(b) and constitute $\sim -3\%$ pressure offset at 2.30 TPa and each term accounts for approximately one third of the total uncertainty at peak pressure. Following these corrections, we provide a third-order Vinet fit to our reduced isentrope and 300 K isotherm in Table I.

Compression rates and time-dependent material response can modify the determined isentrope. It has long been postulated that laser-driven compression rates, when compared to slower compression rates of gas guns and pulsed power machines, would modify the material response and produce systematically stiffer material response. We find that our results and those determined at 20× slower compression rates [5] are in excellent agreement over the full range of measurements (up to 0.45 TPa in the previous work [5].) This agreement over such a wide range of compression rates is consistent with predictions from the Preston-Tonks-Wallace strength model [24] for Cu, which suggests that the strain-rate dependence of the strength of copper is sufficiently small that no observable difference in response would be observed at these rates. Our Letter further validates the accuracy of laser-driven ramp-compression experiments and supports the view that experimental platform discrepancies, which measure the material response on different timescales, are indicative of a rate-dependent response.

We performed DFT simulations to examine the electron density distribution for Cu at 300 K to a maximum density of 27.3 g/cc and show the calculated pressure-density curve (yellow line) in Fig. 2(b). These simulations reproduce well the pressure-induced progressive stiffening of Cu. The spread in the DFT models reported in Fig. 2(b) illustrates the finite range over which the calculations were performed and should serve as a cautionary reminder that extrapolating EOS models outside of the range where the underlying experiments or simulations have been carried out can be misleading.

Previous theoretical work on copper examined the crystal structure stability and the static lattice energy to up to 0.56 [17] and 10 TPa [20] along the room temperature isotherm. In those works, it was found that the fcc structure is most energetically favorable at all pressures. To test the structure predictions of first-principal models, we carried out a series of quasi-isentropic compression experiments coupled with x-ray diffraction to probe the crystal structure

TABLE I. Best-fit parameters for the third-order Vinet fit to the calculated principal isentrope and 298 K isotherm starting at an initial density of 8.939 g/cm^3.

Path	K_o (GPa)	η	β	ψ
Principal isentrope	138.9 ± 0.8	6.05 ± 0.8	2.53 ± 0.4	1.34 ± 0.6
Isentrope upper	123.3 ± 1.5	8.55 ± 0.2	-11.36 ± 0.8	26.83 ± 1.2
Isentrope lower	156.5 ± 0.7	3.48 ± 0.1	17.14 ± 0.3	-25.85 ± 0.4
298 K isotherm	133.6 ± 0.8	6.29 ± 0.8	2.06 ± 0.4	1.65 ± 0.6
Isotherm upper	118.7 ± 1.5	8.77 ± 0.2	-11.78 ± 0.8	27.05 ± 1.2
Isotherm lower	151.4 ± 0.7	3.63 ± 0.6	17.08 ± 0.3	-26.16 ± 0.5

of copper. We combined laser-driven ramp compression and nanosecond x-ray diffraction at the OMEGA laser facility [1] to determine the crystal structure and density of Cu up to ~1.15 TPa.

As shown in Fig. 3(a), the target design consists of a single crystal diamond ablator, a Au preheat shield, a polycrystalline Cu foil, and a diamond window. The target assembly is ramp compressed by seven beams of the OMEGA laser to peak pressures of 570 → 1150 GPa, where laser pulse shaping allows this pressure to be sustained for ~1 ns. During the experiment, we ramp compress the diamond ablator and the diamond window. The Cu sample, placed between the two diamond layers, reverberates and follows a quasi-isentropic compression path. During this pressure hold period, the sample is probed by quasimonochromatic Ge He-α (10.25 keV) or Cu He-α (8.37 keV) x rays as shown in Fig. 3(b). The x ray scatter from interatomic Cu lattice planes with spacings d constructively interfere when the Bragg condition [$n\lambda = 2d\sin(\theta)$] is met and produces a diffraction pattern recorded on x-ray sensitive image plates. By measuring multiple d-spacing diffraction lines [see Fig. 3(c)], we discriminate between different theoretically proposed Cu structures. A more thorough description of the experimental technique can be found elsewhere [25,26].

The results from four x-ray diffraction experiments are shown in Fig. 4 as the cyan circles (see Supplemental Material [27] for tabulated values). Low-pressure static measurements are shown as the white circle and squares. The four most energetically favorable high-pressure phases predicted from first principals (fcc, hcp, 9R, and bcc) are shown. In this Letter, we observed three diffraction peaks that are consistent with the proposed fcc: (111), (200), and (220). This Letter shows that the ambient fcc is stable to pressures up to 1.15 TPa.

Once the crystallographic structure is known, we are able to determine the density state of the Cu from the measured d spacing. Throughout the experiment, a velocity interferometer diagnostic (VISAR) records the wave profiles that are transmitted through the target assembly [see Fig. 3(b)]. Using a wave profile analysis, we determine the pressure state of the sample during the x-ray probe period. The determined P-ρ points from our x-ray diffraction experiments are shown in Fig. 2 as the cyan circle. We find that our pressure-density states from XRD are in good agreement with the isentrope determined from the ramp-compression technique. To date, there has been no direct comparison of the resultant high-pressure P-ρ states determined using the isentropic compression wave reverberation technique [25,26] with an isentrope determined from wave profile analysis [4–7]. The agreement between the independent experimental results presented here confirms that

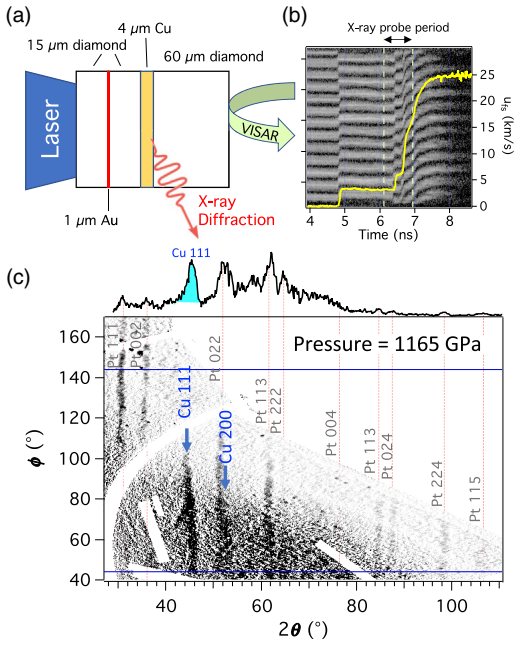

FIG. 3. (a) The target design on the OMEGA laser experiment to measure the crystal structure of Cu to 1200 GPa. [25,26] (b) 1D-VISAR image and extracted diamond free-surface velocity profile which is used to determine sample pressure.(c) X-ray diffraction image for Cu at 1165 GPa projected into 2θ-ϕ angular space, where θ is the scattering angle and ϕ is the azimuthal angle around the incident x-ray direction. The red vertical dotted lines show positions of ambient pressure Pt x-ray diffraction peaks used for diffraction angle calibration. The blue arrow indicates the position of the Cu (111) and Cu (200) fcc peaks.

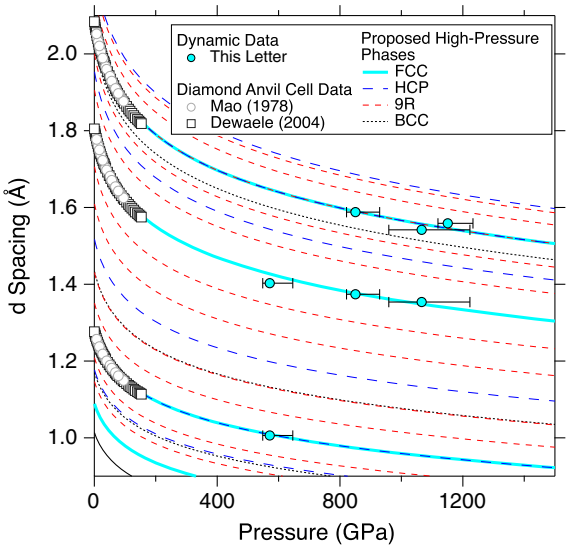

FIG. 4. The d spacing of our experimentally determine diffraction peaks (red points) and low-pressure DAC measurements (white circles and squares) are shown. These data are compared with the fcc, hcp, *9R* and bcc phases, the 4 most energy favorable structures predicted from *ab initio* LDA calculations [17,20]. Our measurements agree with only the fcc phase which DFT predicts to be the most energy favorable energy to 10 TPa.

the diamond layered wave reverberation technique commonly utilized at laser-driven facilities [25] does well to approximate an isentropic loading path.

Our DFT-MD simulations also show that the charge distribution of the Cu $3d$ and $4s$ electrons can be very well approximated by a spherical distribution around the Cu ions. This analysis provides an intuitive microscopic interpretation that at high density (above $\sim$15 g/cc) the atom-in-jellium calculations should capture the compressibility of Cu just as well as the more computationally expensive quantum simulations using DFT-MD. Atom-in-jellium models have a long history in the construction of EOS models over a wider range of density and temperature states, but the cold curves generated using this model have not be benchmarked at high pressure (> 0.5 TPa) [20,48–50]. Throughout the high-pressure regime, the model approach is to approximate the states of the copper as a copper ion in a neutral cell embedded in a uniform electron gas of the correct density. Atom-in-jellium calculations were used to construct a tabular EOS for Cu following the method used previously for several other elements [51,52]. Using this model, the total electronic free energy was calculated, including the cold compression curve, the Debye temperature, and the mean amplitude of thermal vibrations [49].

At peak compression, we find that our atom-in-jellium calculations, as well as the linear combinations of Gaussian type orbitals fitting function method [20] (the stabilized jellium model) reproduces our data well (brown and green lines of Fig. 2). These jellium models require few inputs and assume that the ionic structure can be replaced by an ionic charge distribution with a constant positive-charge background. Further, the only input parameters are the average density of valence electrons and an exchange correlation correction. This method is well suited at high compressions ($\rho_o/\rho < 0.7$) for simple metals as it does not spatially partition between the muffin tin and interstitial regions, and it does not require electronic partitioning between the core and band states. The agreement with our experimental measurements indicate that copper at 2.30 TPa remains an "ideal metal" (the valence electrons can be prescribed as an electron gas) [53].

As a close-packed metal, atom-in-jellium calculations of Cu are expected to be relatively accurate [54]. However, the one-dimensional spherically symmetric treatment of the charge distribution is expected to be less accurate than three-dimensional methods (such as plane wave DFT). In comparisons with other elements, atom-in-jellium calculations have generally been found to be much less accurate than 3D DFT at pressures below $\sim$0.5–1.0 TPa. Where atom-in-jellium calculations are observed to be satisfactory, this seems not to be because they are more accurate in absolute terms so much as that the inaccuracy becomes proportionately less with respect to the density. At high compressions and temperatures, the advantages of the atom-in-jellium method also become more pronounced: calculations are much faster than 3D methods, while also treating all the electrons explicitly (avoiding the limitations of pseudopotential DFT).

The spherically symmetric atom-in-jellium representation used for the electron wave functions is obviously not capable of representing states in condensed matter accurately enough to capture differences between solid phases and have been found to be much less accurate than multiatom calculations around ambient conditions [51]. One interpretation of their relative accuracy at terapascal pressures is that the inaccuracy around ambient, considered as a pressure and energy discrepancy, is simply proportionally smaller at high pressures. However, recent studies of warm, dense matter have found that the electrons experience an effective screened Yukawa potential [52], and thus the atom-in-jellium representation may be relatively accurate as opposed to merely less inaccurate. Our measurements on Cu to 2.3 TPa experimentally support this view.

In conclusion, we used ramp-compression techniques to examine the material response and crystal structure of copper to unprecedented conditions. We measured the isentrope to 2.30 TPa and combined ramp compression with nanosecond x-ray diffraction techniques to probe the crystalline structure. We find that the fcc phase is most stable across this pressure range, as predicted, and that the simplified stabilized jellium model reproduces these results well. The simple response of copper under dynamic compression and the ability to accurately model the Hugoniot and isentrope using first-principals calculations suggest that copper is an excellent pressure standard candidate over a wide region of phase space.

This work was performed under the auspices of the U.S. Department of Energy by Lawrence Livermore National Laboratory under Contract No. DE-AC52-07NA27344.

*Corresponding author.
Frataduono1@LLNL.Gov

[1] T. R. Boehly, R. S. Craxton, T. H. Hinterman, J. H. Kelly, T. J. Kessler, S. A. Kumpan, S. A. Letzring, R. L. McCrory, S. F. B. Morse, W. Seka, S. Skupsky, J. M. Soures, and C. P. Verdon, Rev. Sci. Instrum. **66**, 508 (1995).
[2] C. A. Hall, M. D. Knudson, J. R. Asay, R. Lemke, and B. Oliver, Int. J. Impact Eng. **26**, 275 (2001).
[3] E. I. Moses, R. N. Boyd, B. A. Remington, C. J. Keane, and R. Al-Ayat, Phys. Plasmas **16**, 041006 (2009).
[4] S. D. Rothman, J.-P. Davis, J. Maw, C. M. Robinson, K. Parker, and J. Palmer, J. Appl. Phys. **38**, 733 (2005).
[5] R. G. Kraus, J.-P. Davis, C. T. Seagle, D. E. Fratanduono, D. C. Swift, J. L. Brown, and J. H. Eggert, Phys. Rev. B **93**, 134105 (2016).
[6] R. F. Smith, J. H. Eggert, R. Jeanloz, T. S. Duffy, D. G. Braun, J. R. Patterson, R. E. Rudd, J. Biener, A. E. Lazicki, A. V. Hamza, J. Wang, T. Braun, L. X. Benedict, P. M.

Celliers, and G. W. Collins, Nature (London) **511**, 330 (2014).
[7] R. Smith, D. Fratanduono, D. Braun, T. Duffy, J. Wicks, P. Celliers, S. Ali, A. Fernandez-Pañella, R. Kraus, D. Swift, G. Collins, and J. Eggert, Nat. Astron. **2**, 452 (2018).
[8] P. M. Celliers, D. K. Bradley, G. W. Collins, D. G. Hicks, T. R. Boehly, and W. J. Armstrong, Rev. Sci. Instrum. **75**, 4916 (2004).
[9] R. Fowles and R. F. Williams, J. Appl. Phys. **41**, 360 (1970).
[10] M. Cowperthwaite and R. Williams, J. Appl. Phys. **42**, 456 (1971).
[11] J. Cagnoux, P. Chartagnac, P. Hereil, M. Perez, and L. Seaman, Ann. Phys. (N.Y.) **12**, 451 (1987).
[12] J. B. Aidun and Y. M. Gupta, J. Appl. Phys. **69**, 6998 (1991).
[13] P. I. Dorogokupets, T. S. Sokolova, B. S. Danilov, and K. D. Litasov, Geodin. tektonofiz. **3**, 129 (2015).
[14] Y.-B. Liu, X.-S. Li, Y.-L. Feng, Y.-L. Cui, and X. Han, Physica (Amsterdam) **394B**, 14 (2007).
[15] R. Joshi, N. Bhatt, B. Thakore, P. Vyas, and A. Jani, Comput. Condens. Matter **15**, 79 (2018).
[16] W. Xiao-Lu, G. Xiang, M. Gui-Cun, Y. Jun, Z. Wen-Qing, and L. Jia-Ming, Chin. Phys. Lett. **25**, 3350 (2008).
[17] B. Li-Gang and L. Jing, Chin. Phys. Lett. **27**, 036403 (2010).
[18] A. E. Gheribi, J.-M. Roussel, and J. Rogez, J. Phys. Condens. Matter **19**, 476218 (2007).
[19] W. B. Holzapfel, High Press. Res. **30**, 372 (2010).
[20] C. Greeff, J. Boettger, M. Graf, and J. Johnson, J Phys. Chem. Solids **67**, 2033 (2006).
[21] C. Bercegeay and S. Bernard, Phys. Rev. B **72**, 214101 (2005).
[22] A. Dewaele, P. Loubeyre, and M. Mezouar, Phys. Rev. B **70**, 094112 (2004).
[23] G. R. Fowles, J. Appl. Phys. **32**, 1475 (1961).
[24] D. L. Preston, D. L. Tonks, and D. C. Wallace, J. Appl. Phys. **93**, 211 (2003).
[25] J. R. Rygg, J. H. Eggert, A. E. Lazicki, F. Coppari, J. A. Hawreliak, D. G. Hicks, R. F. Smith, C. M. Sorce, T. M. Uphaus, B. Yaakobi, and G. W. Collins, Rev. Sci. Instrum. **83**, 113904 (2012).
[26] A. Lazicki, J. R. Rygg, F. Coppari, R. Smith, D. Fratanduono, R. G. Kraus, G. W. Collins, R. Briggs, D. G. Braun, D. C. Swift, and J. H. Eggert, Phys. Rev. Lett. **115**, 075502 (2015).
[27] See Supplemental Material at http://link.aps.org/supplemental/10.1103/PhysRevLett.124.015701 for details of the analysis and methods, which includes Refs. [28–47].
[28] T. J. Ahrens, *High-Pressure Shock Compression of Solids*, edited by J. R. Asay and M. Shainpoor (Springer-Verlag, New York, 1993), p. 75.
[29] S. P. Lyon and J. D. Johnson, Los Alamos National Laboratory, Los Alamos, NM, Report No. LA-UR-92-3407, 1992.
[30] R. Hill, *The Mathematical Theory of Plasticity* (Clarendon Press/Oxford University Press, New York/Oxford, 1950).
[31] R. F. Smith, J. H. Eggert, R. E. Rudd, D. C. Swift, C. A. Bolme, and G. W. Collins, J. Appl. Phys. **110**, 123521 (2011).
[32] J. M. Brown and R. G. McQueen, J. Geophys. Res. **91**, 7485 (1986).
[33] G. I. Taylor and H. Quinney, Proc. R. Soc. A **143**, 307 (1934).
[34] D. Erskine, AIP Conf. Proc. **1793**, 160017 (2017).
[35] S. Nosè, J. Chem. Phys. **81**, 511 (1984).
[36] P. E. Blöchl, O. Jepsen, and O. K. Andersen, Phys. Rev. B **49**, 16223 (1994).
[37] G. Kresse and J. Furthmüller, Phys. Rev. B **54**, 11169 (1996).
[38] J. P. Perdew and A. Zunger, Phys. Rev. B **23**, 5048 (1981).
[39] D. M. Ceperley and B. J. Alder, Phys. Rev. Lett. **45**, 566 (1980).
[40] J. P. Perdew, K. Burke, and M. Ernzerhof, Phys. Rev. Lett. **77**, 3865 (1996).
[41] H. K. Hieu and N. N. Ha, AIP Adv. **3**, 112125 (2013).
[42] D. Hayes, R. Hixson, and R. McQueen, AIP Conf. Proc. **505**, 483 (2000).
[43] J. Wang, R. F. Smith, J. H. Eggert, D. G. Braun, T. R. Boehly, J. R. Patterson, P. M. Celliers, R. Jeanloz, G. W. Collins, and T. S. Duffy, J. Appl. Phys. **114**, 023513 (2013).
[44] J. K. Wicks, R. F. Smith, D. E. Fratanduono, F. Coppari, R. G. Kraus, M. G. Newman, J. R. Rygg, J. H. Eggert, and T. S. Duffy, Sci. Adv. **4**, eaao5864 (2018).
[45] P. Dorogokupets and A. Oganov, in *Doklady Earth Sciences* (Springer, New York, 2006), Vol. 410, p. 1091.
[46] D. J. Steinberg, S. G. Cochran, and M. W. Guinan, J. Appl. Phys. **51**, 1498 (1980).
[47] C. A. McCoy, M. D. Knudson, and S. Root, Phys. Rev. B **96**, 174109 (2017).
[48] R. M. More, K. H. Warren, D. A. Young, and G. B. Zimmerman, Phys. Fluids **31**, 3059 (1988).
[49] D. A. Liberman and B. I. Bennett, Phys. Rev. B **42**, 2475 (1990).
[50] L. X. Benedict, K. P. Driver, S. Hamel, B. Militzer, T. Qi, A. A. Correa, A. Saul, and E. Schwegler, Phys. Rev. B **89**, 224109 (2014).
[51] D. C. Swift, T. Lockard, R. G. Kraus, L. X. Benedict, P. A. Sterne, M. Bethkenhagen, S. Hamel, and B. I. Bennett, Phys. Rev. E **99**, 063210 (2019).
[52] D. C. Swift, T. Lockard, O. Heuze, M. Frost, S. Glenzer, K. J. McClellan, S. Hamel, J. E. Klepeis, L. X. Benedict, P. A. Sterne, and G. J. Ackland, arXiv:1909.05391.
[53] H. B. Shore and J. H. Rose, Phys. Rev. Lett. **66**, 2519 (1991).
[54] D. A. Liberman, Phys. Rev. B **20**, 4981 (1979).